New Jersey Institute of Technology

Digital Commons @ NJIT

Spring 5-31-2013

Effect of scan time on resting state parameters

Dhruti Patel
New Jersey Institute of Technology

Follow this and additional works at: https://digitalcommons.njit.edu/theses

Part of the Biomedical Engineering and Bioengineering Commons

ABSTRACT

EFFECT OF SCAN TIME ON RESTING STATE PARAMETERS

by

Dhruti Patel

In the past decade the interest in studying the spontaneous low-frequency fluctuations (LFF) in a resting-state brain has steadily grown. By measuring LFF (< 0.08 Hz) in blood-oxygen-level-dependent (BOLD) signals, resting-state functional magnetic resonance imaging (rs-fMRI) has proven to be a powerful tool in exploring brain network connectivity and functionality. Rs-fMRI data can be used to organize the brain into resting state networks (RSNs). In this thesis, rs-fMRI data are used to determine the minimum data acquisition time necessary to detect local intrinsic brain activity as a function of both the amplitude of low frequency fluctuations (ALFF) and the fractional amplitude of low frequency fluctuations (fALFF) in BOLD signals in healthy subjects. The data are obtained from 22 healthy subjects to use as a baseline for future rs-fMRI analysis. Voxel-wise analysis is performed on the whole brain, gray matter volume, and two previously established RSNs: the default mode network (DMN) and the visual system network, for all the subjects in this study.

Pearson's correlation coefficients (r-values) are calculated from each subject. The entire time series for one subject is divided into 31 subsections and the r-values are calculated between each consecutive subsection in a subject. In total, there are 30 r-values. To better understand what the results mean across subjects and within subjects Fisher transformations are applied to the 30 calculated r-values for each subject to get a normal z-distribution. The mean across 22 subjects' z-values is calculated for group

analysis. In the end, there are 30 mean values. Finally, an exponential curve fit model is calculated across the 22 subjects using the calculated mean values, and an asymptotic growth model is used to detect the minimum data acquisition time required to obtain both ALFF and fALFF of the BOLD signals at rest. The results show that the minimum time required to detect an ALFF and fALFF of the BOLD signals at rest is 12 and 13.33 minutes respectively. Future studies can focus on determining the minimum scanner time using similar analysis for different physiological states of the brain.

EFFECT OF SCAN TIME ON RESTING STATE PARAMETERS

by
Dhruti Patel

A Dissertation
Submitted to the Faculty of
New Jersey Institute of Technology
in Partial Fulfillment of the Requirements for the Degree of
Master of Science in Biomedical Engineering

Department of Biomedical Engineering

May 2013

.

BIOGRAPHICAL SKETCH

Author: Dhruti Patel

Degree: Master of Science

Date: May2013

Undergraduate and Graduate Education:

- Master of Science in Biomedical Engineering,
  New Jersey Institute of Technology, Newark, NJ, 2013

- Bachelor of Science in Biomedical Engineering,
  Rutgers State University, New Brunswick, NJ, 2012

Major: Biomedical Engineering

This thesis is dedicated to my lovely family.

ACKNOWLEDGMENT

I would like to thank my thesis advisor, Dr. Bharat B. Biswal, for guiding me through all the ups and downs I encountered throughout the duration of this thesis. I also want to thank my committee members Dr. Di and Dr. Alvarez for giving me a clear direction to reach my end goal and providing different approaches throughout the whole process. To be honest, this thesis would not have been possible without the dedication and encouragement from my committee.

I want to thank the Brain Connectivity Lab in the Department of Biomedical Engineering at NJIT for helping me get started with my thesis. Without their assistance at learning a new field in BME I would not have made it this far in my master's thesis. They are the building blocks for my thesis. Thank you so much for accepting me into your home. Special thanks to Suril Gohel!

Lastly, I want to thank my family for being patient with me while writing up this thesis. Big thanks to Mathew Yarossi for helping me solve any dilemmas.

TABLE OF CONTENTS

TABLE OF CONTENTS

(Continued)

LIST OF TABLES

LIST OF FIGURES

Abbreviations:

MRI	Magnetic Resonance Imaging
fMRI	functional MRI
NMR	Nuclear magnetic resonance
LFOs	Low-Frequency Oscillations
LFF	Low-Frequency Fluctuations
ALFF	Amplitude LFF
fALFF	fractional ALFF
BOLD	Blood-Oxygen-Level-Dependent
Rs-fMRI	Resting-State functional Magnetic Resonance Imaging
ROIs	Region of Interests
RSNs	Resting State Networks
DMN	Default Mode Network
AD	Alzheimer's disease
PET	Positron emission tomography
FFT	Fast Fourier transform
TR	Time repetition
RF	Radio frequency
BW	Bandwidth
EPI	Echo planar imaging
TE	Echo time
HRF	Hemodynamic response function
ICA	Independent component analysis

CHAPTER 1

INTRODUCTION

1.1 Preliminary Research

Functional magnetic resonance imaging (fMRI) is another branch of magnetic resonance imaging (MRI). Both of these modalities are non-invasive methods of brain imaging utilizing a strong magnetic field (usually a magnetic field strength of 3 Tesla). They also incorporate several radio frequency pulses to acquire either structural or functional images of the brain. Unlike MRI, which only gives high-resolution anatomical images of the brain, fMRI is able to detect brain activity and behavior with low-resolution structural images of the brain. To study the brain function, most studies measure task-related changes in the local hemodynamic activity within each region by measuring the blood oxygenation-level dependent (BOLD) signal. The current study focuses on the neural activity and BOLD signal at rest, without the stimulus of a task.

Positron emission tomography (PET) imaging is similar to fMRI; it gives functional information of the brain. However, instead of measuring differences in magnetic property of used vs. unused blood, PET imaging measures blood flow by tracking the distribution of an injected positron-emitting tracer. PET imaging technique is more invasive and provides poorer spatial and temporal resolution than fMRI [1].

As previously stated, this particular study focuses on resting-state fMRI (rs-fMRI). The BOLD signal obtained from an fMRI study is in time domain but once converted into frequency domain it provides a statistically significant temporal correlation between regions of the brain that are active and lack direct anatomical

projections known as functionally connected regions. The reconstruction of the signal in the frequency domain is accomplished with Fourier transform (FT) and band pass filtered to specific frequency bands (0.01-0.1 Hz). The filter is set to these numbers to remove noise artifacts and other components underlying the BOLD signal, such as cardiac or respiratory components. Rs-fMRI studies look at the intrinsic properties of the brain; so the functionally connected regions observed at rest are correlated through their synchronous BOLD signals.

Over the years, these synchronous BOLD signals between regions that are spatially distinct have been examined to identify resting state networks (RSNs). The most fundamental RSN is the default mode network (DMN). There are seven more RSNs that have been identified based on different mental processes at rest. These seven RSNs are also detected during the onset of a particular task [2-4].

1.2 Overview

Although most rs-fMRI studies are focused on the examination of temporal correlations between low-frequency oscillations (LFOs) in BOLD signal, the current study explores the amplitude information in these BOLD signals. Specifically, this study focuses on the total power within the low frequency range using amplitude low frequency fluctuations (ALFF) and fractional ALFF (fALFF) as reliable indices for local intrinsic brain activity in healthy people. The ALFF and fALFF measurements in each voxel can be used to detect the RSNs. Individual variability in these measurements have been linked to changes in neural activation and behavior [5].

Rs-fMRI experiment is also a preferable method for clinical studies to look at brain system integrity patterns as a powerful tool for detecting differences among healthy

people and people suffering from neurological and psychiatric disorders. Changes in either ALFF or fALFF values in each voxel for different regions of interest (ROIs) within the brain have also been reported for a number of neuropsychiatric disorders, including autism, depression, attention deficit hyperactivity disorder, and schizophrenia [6].

1.3 Objective

The aim of this study is to determine the minimum amount of scan time necessary to obtain viable rs-fMRI data from healthy subjects. Viable data is defined here as data that features the ideal ALFF and fALFF values from the BOLD signal at rest. The ideal values are the values that remain constant after reaching a certain measurement of ALFF and fALFF for different ROIs. The main reasons to study the rs-fMRI are it does not involve active participation from the subject, it can be performed on coma induced or sedated patients, and it creates a set baseline for all the participants. The reason to study the minimum resting state scan time is because for each hour the subject is in the scanner for; it costs the Principal Investigator (PI) of the study at least $500. Also, the longer the subject is in the scanner, greater the possibility for head motion by the subject and this decreases the chance of any significant statistical analysis on this data.

In this study, 22 healthy subjects were scanned for 41 minutes each to acquire their rs-fMRI data. While the subject is in the scanner, several low-resolution images of the brain are taken at a specified repetition time (TR) between each image. In this study, the TR between each image is 2.5 seconds.

Next, the time series from each subject is divided into different subsections or runs. Each subject ends up with 31 different subsections within the 995 pre-processed time series. Spatial maps of the ALFF and fALFF measurements are calculated for each

subject's subsection. Then using these spatial maps, Pearson's correlation coefficients (r-values) are calculated between each consecutive subsection for each subject. Each subject now has 30 different calculated r-values. Finally, group level and inter-subject analysis are performed on the calculated r-values to determine the minimum resting state scan time for different ROIs.

1.4 Outline

This thesis analyzes rs-fMRI data taken from 22 healthy subjects who are in the MRI scanner for about 41 minutes each. Chapter 2 goes into detail about MRI neuroimaging technique. The following chapter describes fMRI modality. Chapter 4 goes over the methods performed in this study. Chapter 5 and 6 talk about results and conclude the study, respectively.

CHAPTER 2

MAGNETIC RESONANCE IMAGING

Magnetic Resonance Imaging (MRI) is similar to nuclear magnetic resonance (NMR). NMR describes the precession when a certain nuclei placed in a strong magnetic field resonates at radiofrequencies (RF) described by the Larmor frequency specific to that atom. The Larmor frequency depends on the strength of the external magnetic field (B_0) and an intrinsic property of the nucleus, the gyromagnetic ratio [7]. The decay rate of the signal detected from a sample depends on the relaxation time constants T1 and T2 after the atom has been excited.

The image contrasts are detected by localized variation in the tissue relaxation time constants. The use of additional magnetic field gradients is required to allow spatial localization of the signal detected by altering the Larmor frequency of Hydrogen atom in water molecules depending on their location in the field. Thus MRI similar to NMR is an acceptable modality to study the anatomy of the brain and to diagnose different diseases by providing great tissue contrast using different types of pulse sequences.

2.1 Overview of MRI

Nuclear magnetic resonance is a method to observe the magnetic properties of different materials when the nuclei are immersed in a static magnetic field (B_0) and exposed to the RF pulse. The magnetic property depends on the spin associated with the nuclei of that material; every nuclei posses a spin of +1/2 and -1/2, this spin generates a magnetic field, thus hydrogen protons have magnetic moments. MR imaging is predominantly concerned with the signal detection from hydrogen nuclei in water molecules, constituting 70% of body weight, 70.6% of gray matter, and 84.3% of white matter in the brain. The hydrogen

nucleus has only one proton and this aligns either in parallel or anti-parallel direction with the B_0 [8]. The interaction of the magnetic moment (+/- ½) of the hydrogen proton with B_0 causes the proton to precess (circular rotary motion) around the magnetic field.
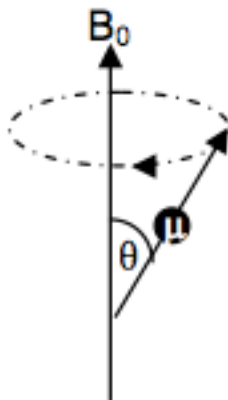
Figure 2.1 The precession of a proton in a strong magnetic field. Θ is the angle between the spinning magnetic moment (μ) and the external magnetic field (B_0).

The speed of rotation (precession) is given by the Larmor equation

$$v_0 = \gamma\, B_0\, /\, 2\pi \qquad\qquad (2.1)$$

where v_0 is the Larmor frequency (Hz), γ is the gyromagnetic ratio (hydrogen = 42.58 MHz / T), and B_0 is the external magnetic field in Tesla (T) [9].

2.2   Static Magnetic Field

The static external magnetic field (B_0) is usually in the range from 1.5T to 3.0T and is applied in positive z direction perpendicular to x-y axis. The hydrogen protons align in parallel with the direction of B_0 (lower energy state) or anti-parallel with B_0 (higher energy state). In the absence of Bo these states have equal energy. In the presence of Bo a proton in the state $E\uparrow$ (lower energy) can switch to the state $E\downarrow$ (higher energy) by absorbing a photon with energy equal to equation 2.2.

$$E\downarrow - E\uparrow = h\gamma\, B_0\, /\, 2\pi \qquad\qquad (2.2)$$

Where h is Planck's constant and the Larmor frequency is proportional to gyromagnetic ratio and B_0. The B_0 allows the protons to have zero net magnetization in x-y direction because per every 1T there is 0.1% of hydrogen protons that are aligned parallel (precessing) to B_0. As the magnetic field strength increases, more and more protons align parallel to B_0 [10].

2.3 RF Pulse

Sending alternating currents in two coils positioned along the x and y direction generates the electromagnetic RF pulse. The dynamic equilibrium is disturbed through the transmission of photons with the Larmor frequency as described by equation 2.1; applying a 90° pulse for a short period excites the protons. The angle between the z-axis and M is called the flip angle (equation 2.3),

$$\theta = \gamma B_1 t \tag{2.3}$$

where θ= flip angle, γ= Gyromagnetic ratio, B_1 = External Magnetic Field (RF pulse), t= duration of RF pulse. The net magnetization vector has both a longitudinal (z direction) and transverse (x-y plane) component as the protons precess at a fast rate once excited by the RF pulse. When the RF pulse is switched off, the system returns to its dynamic equilibrium (relaxation process) oscillating around the new Larmor frequency around M. The transverse component returns to zero, and the longitudinal component becomes M_o again, the return to equilibrium is called relaxation.

To summarize the excitation process, the protons are excited by the RF pulse and the transverse component of the net magnetization vector in each voxel rotates clockwise at the precession frequency in the stationary reference frame. This induces an alternating current in an antenna (coil) placed around a person's head in the xy-plane. Depending on

7

the level of excitation, different relaxation images are detected. This is described by figure 2.2 [10].
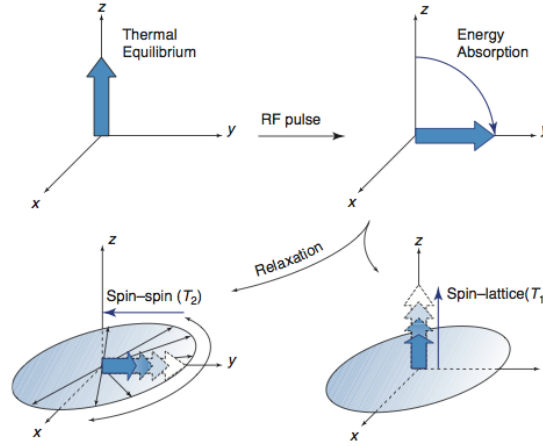
Figure 2.2 Overview of NMR experiment. [10]

The decay of M_{xy} (transverse magnetization vector) is defined by T_2 relaxation time causing the disappearance of the transverse component of the net magnetization vector. T_2 can be defined as the time taken by M_{xy} to reduce to 37% of its original value due to both magnetic field in homogeneities and spin-spin interactions. The relationship between decay of M_{xy} and T_2 is given by equation 2.4.

$$M_{xy}(t) = M_0 \, e^{-t/T2} \tag{2.4}$$

Where M_0 is the value of the transverse component immediately after the RF pulse and T_2= transverse relaxation time.

The T_1 relaxation time is related to the regeneration of longitudinal magnetization vector M_z. This is defined as the time taken by longitudinal magnetization vector M_z to recover 63% of its original value after application of RF pulse. T_1 relaxation time depends on the external magnetic field: the higher the field, the higher T_1. Equation 2.5 gives the relationship between M_z and T_1 at any instantaneous time t.

$$M_z(t) = M_o(1 - e^{t/T1}) \qquad (2.5)$$
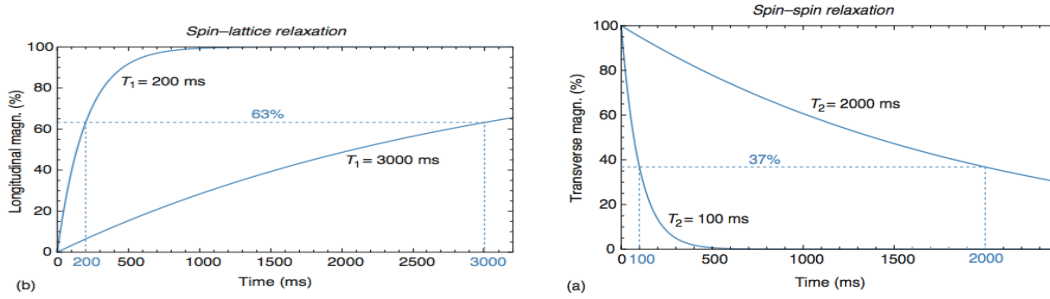
Figure 2.3 T_1 & T_2 relaxation times for CSF and fat with a flip angle of 90.

2.4 Image Acquisition

To create images, the scanner uses a series of changing magnetic gradients and oscillating electromagnetic fields, known as a pulse sequences. The images are constructed using both the frequency and phase encoding information of the hydrogen atom. On T1-contrast images, fluid appears as black, gray matter appears as dark gray, and white matter appears as light gray. However, on T2- contrast images, the gray matter is light, white matter is dark, and fluid is very bright. The ability to distinguish different locations within an image is known as spatial resolution. Since MR images sample the brain in three dimensions, the basic sampling units of MRI are known as voxels or volume elements. As the voxel size decreases, the ability to identify fine structure in a brain image improves. Although, structural MR images are considered to be static representation of the brain, fMRI is inherently dynamic, in that it measures changes in brain activity over time. The rate at which a technique acquires images or its sampling rate, determines its temporal resolution [11]. Therefore, fMRI samples the brain in four dimensions; the fourth dimension is the different number of images generated in the MRI scanner.

In order to get the right spatial resolution, the magnetic field must be spatially dependent. A series of linear magnetic field gradients in the x, y, and z-directions are superimposed onto the z-component of the B_0 field. As the gradients change, the scanner produces noise that needs to be canceled with earplugs. The Gz-gradient selects the number of slices needed to cover the whole brain in one image. The dimensions are in units of mm. As a result, the new Larmor frequency becomes equation 2.6.

$$\omega\ (z)= \gamma\ (B_0 +G_z\ z) \tag{2.6}$$

The thickness of the selected slice is defined by equation 2.7.

$$\Delta z= \Delta\omega/ \gamma\ G_z = BW/ \gamma\ G_z \tag{2.7}$$

The slice thickness is proportional to the bandwidth (BW) of the RF pulse and inversely proportional to the G_z. The minimum slice thickness used is typically 1mm on a 3T imaging system [10].

The next step is the phase encoding gradient, which causes a change in the precession frequency of individual columns for a particular time. Once it is turned off, the precession frequencies in the columns are same. However, the term phase encoding arises from the fact that not all columns precess at the same frequency. The last step is the frequency-encoding gradient applied only during the time of signal readout or when the RF pulse is ON. Each pixel in an individual column has the same phase difference but slightly different precession frequency.

To understand how and in which order the three different gradients have to be applied to sample the whole Fourier space, the k-theorem is used. It states that for a given data point in k-space (kx, ky), its signal S (kx, ky) is the sum of all the little signal from

each voxel (x, y) in the physical space, under the gradient field. The acquired MR signal, in 2-D space, is the Fourier transform of the imaged object.

(a)   (b)
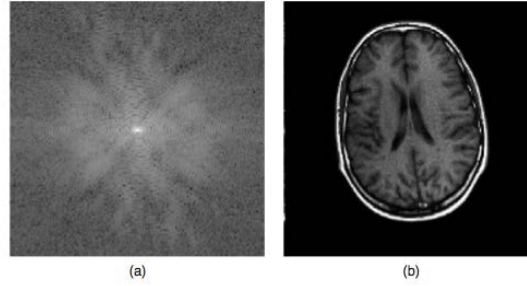
Figure 2.4 Illustration of K-theorem. (a) The raw data measured by the MR Imaging system. (b) Modulus of the image obtained from a 2D inverse FT of the raw data.

To measure k-space, the 2D spin-echo pulse sequence is demonstrated by figure 2.5.
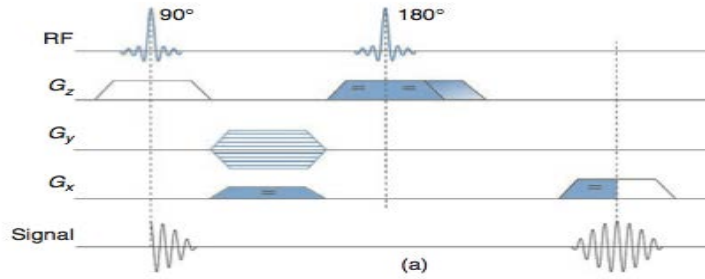
Figure 2.5 Gradient echo pulse sequence [10].

In order to obtain an image, the complete k-space is sampled and the inverse FT is then calculated. To understand the function of the brain, images need to be acquired very rapidly, at approximately the same rate as the physiological changes of interest. For this reason, fast pulse sequences have been developed sensitive to T2* contrast relaxation times, providing high temporal resolution study of functional changes in human brain through fMRI. T2* is the time constant associated with the loss of phase coherence among spins oriented at an angle to the B_0 field. Echo planar imaging (EPI) is a method where the entire k-space is filled using rapid gradient switching pattern following a single excitation of the RF pulse.

11
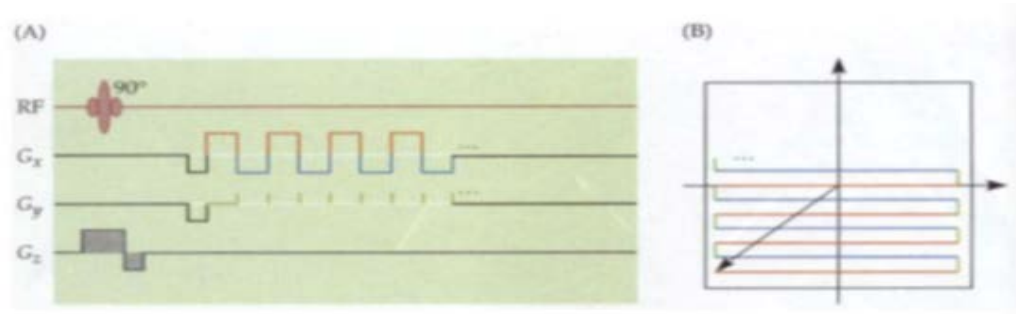
Figure 2.6 EPI pulse sequence and its K-space trajectory [11]

2.4.1 Image Types

Based on the type of contrast involved, MRI images can divide into three types; T1 weighted images, T2 weighted images, and proton density images. All these types of images differ from each other in terms of tissue contrast and values of TR and TE.

T1 weighted images define the contrast between different tissues due to differences in longitudinal relaxation time. A short TR and short echo delay time (TE) is required to acquire T1 images. For T2 weighted images the TR and TE are chosen as to reduce the differences of longitudinal relaxation time T1 and to increase the differences in transverse relaxation time T2 between tissues. The last type of images, proton density detects differences in proton density between two tissue types. This is mainly due to the differences in water content. Table 2.1 summarizes TR and TE for three MRI image types.

Table 2.1 TR and TE times for different weighted images.

Type	Repetition time TR	Echo time TE
ρ-weighted	long	short
T_1-weighted	short	short
T_2-weighted	long	long

2.4.2 MRI Signal

The MRI signal is generated in time domain; however, it is best analyzed in the frequency domain. Fourier transform is a method the converts the signal from time domain to frequency domain. From plot of signal intensity vs. time to signal intensity vs. frequency, resulting in a peak for each resonance frequency of nuclei in the sample [9].

CHAPTER 3

FUNCTIONAL MAGNETIC RESONANCE IMAGING (FMRI)

3.1 Background on fMRI

In the past two decades, fMRI has gained widespread acceptance as a powerful tool for mapping brain function [12]. It is used to quantify physiological changes taking place in the brain over time by analyzing the BOLD signal. The BOLD signal gives information about the brain activity either at rest or while performing a task. The signal is used to detect functional connectivity patterns, RSNs, reflecting the intrinsic energy demands of neuron population that, via firing together with a common functional purpose, have subsequently wired together through synaptic plasticity. The focus of the current thesis is to look into the influence of time on rs-fMRI BOLD signals at LFOs amplitude information at rest.

3.1.1 BOLD Signal

Ogawa et al., was the fist one to analyze fMRI images with BOLD contrast with the idea that changes in blood oxygenation could be measured. BOLD contrast has its origin in the fact that when normally diamagnetic oxygenated hemoglobin gives up its oxygen, it results in deoxygenated hemoglobin that is paramagnetic. The effect of paramagnetic molecules in blood produces a difference in magnetic susceptibility between the blood vessels and the surrounding tissue creating a darker image [13]. The paramagnetic property distorts the magnetic field causing spin de-phasing, resulting in a decay of transverse magnetization, which depends on the time constant T2*. Therefore, MR pulse

sequences sensitive to T2* show more MR signal where blood is highly oxygenated and less MR signal where blood is highly deoxygenated as illustrated by figure 3.1 [11].
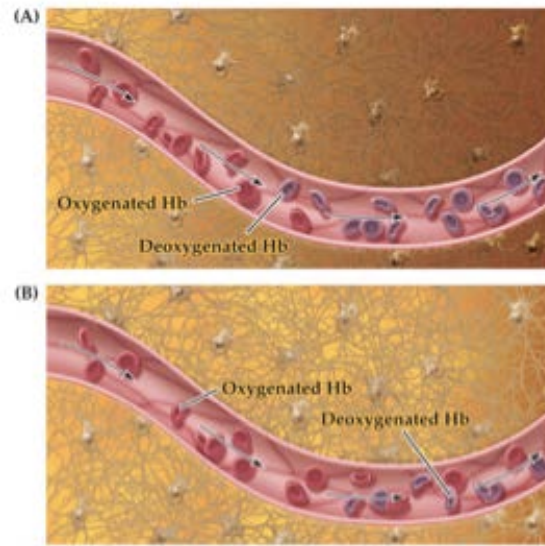
Figure 3.1 Summary of BOLD signal generation [11].

The BOLD signal reflects changes in blood flow, blood volume, and oxygen consumption; these are the physiological changes associated with the BOLD signal. At the onset of a task, the active neurons require two metabolites, oxygen and glucose, to provide the energy for restoration of their membrane potentials. However, these metabolites are not stored locally but are rather delivered through the vascular system, which sends more blood to regions of the brain that are active. Because the blood supplies more oxygen than can be used by the neurons, the result is a systematic increase in blood oxygenation in more active brain regions, which in turn leads to an increase in these regions' BOLD signals. To sum it up, the change in deoxygenated hemoglobin effects the active brain regions' BOLD signals [11].

3.1.2 Hemodynamic Response Function

Over the years, scientists have attempted to capitalize on the spatial temporal dynamics of the hemodynamic response. The spatial temporal dynamics was first observed at the onset of a neural activity where a small rise in deoxygenated hemoglobin peaked at 4 seconds (initial dip) and decreasing several seconds after the termination of the stimulation. The initial dip was believed to originate due to an increase in metabolism before the hemodynamic response kicked in [14]. The hemodynamic response function (HRF) (figure 3.2) illustrates the concentration of oxygenated hemoglobin when the neurons are active and it can be used as an impulse function to find the output of unknown signal. The variation in the BOLD signal across regions result from neural activity related to stimulus and vascular factors [15].
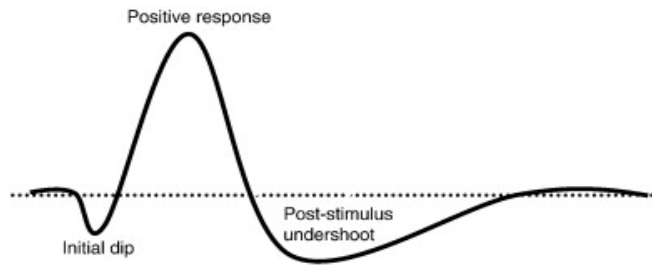
Figure 3.2 The hemodynamic response function (neuronal activity) [14].

3.1.3 Components of BOLD Signal

Raw BOLD signals' time courses, continuous over time, are noisy due to scanner artifacts, motion, and physiological noises such as cardiac and respiratory cycle. As a result of the spurious noise, multiple preprocessing steps are typically used to increase signal to noise ratio to detect the frequency at which the BOLD signal occurs [6]. The

BOLD fluctuations that produce correlations within functional networks occur within a range of 0.01-0.08 Hz, useful for understanding the intrinsic process at rest [3, 16]. Thus, this avoids any positive correlation between regions unlikely to be functionally connected [17].

LFOs have gained increased attention and researchers have identified spontaneous low frequency fluctuations (LFF) in the 0.01-0.1 Hz during both resting and active-task conditions. The information derived from LFO amplitude gives meaningful differences among brain regions; however, several physiological and neural factors can impact LFO amplitudes. To understand why the spontaneous BOLD fluctuations occur at .01-.08 Hz, Zuo et al. [18] subdivided the low frequency range into four bands: slow 5 (.01-.027 Hz), slow 4 (.027-.073 Hz), slow 3 (.073-.198 Hz) and slow 2 (.198-.25 Hz). It was observed that for both ALFF and fALFF measures, slow 4 and slow 5 oscillations were detected within gray matter and slow 2 and slow 3 were restricted to white matter. Respiratory and aliased cardiac signals fall in the range of slows 2 and 3 which are not important [18].

3.2 Two Types of fMRI Experiments

Areas of the brain that exhibit BOLD signal fluctuations at low frequencies (<0.1 Hz) linked in time are assumed to be functionally connected. Measuring the amplitude of resting-state BOLD fluctuations calculated in the low-frequency band and determining the time when these values level out can help detect connectivity patterns in healthy subjects.

3.2.1 Task-Based fMRI

The current understanding of brain function using fMRI has been focused on task-based or stimulus-driven paradigm. Using the relative changes from baseline in the BOLD

signal during the performance of a task or in response to a stimulus, the active brain region during that task is identified [2]. The results acquired from the present study would not be relevant to task-based fMRI because someone performing a finger-tapping task would not need to be in the scanner for an equivalent amount of time.

3.2.2 Resting-state fMRI

The second type of fMRI scan is the resting-state fMRI scan. This particular type of scan looks at the brain when it's at rest, the brain under normal physiological condition remains neuro-electrically and metabolically active [12]. Studies have stated that brain at rest consumes about 90% of brain's energy while brain during task-evoked activity only consumes about 5% of brain's energy.

3.2.2.1 Analysis on Rs-fMRI

Rs-fMRI BOLD signal can be used to detect functional connectivity patterns as discovered by Biswal et al. They demonstrated that under resting conditions, the BOLD signal fluctuations that are measured in the left sensorimotor cortex, become interconnected with fluctuations in the contralateral sensorimotor cortex, in the right supplementary motor area and in right premotor areas, a set of regions constituting the sensorimotor network [16]. Several researchers since then have confirmed that many of the networks engaged during various cognitive tasks are also recognizable during resting state scan [19]. Spontaneous activity in the LFF range is observed across various behavioral states including resting state condition, task performances, and different consciousness states including sleep, anesthesia, and in disorders of consciousness. These spontaneous fluctuations at rest are a representation of different memory, thinking, or intrinsic processes [12].

Cordes et al., studied the rs-fMRI to identify brain regions that show activation on rs-fMRI maps using correlation coefficient analysis. They showed that functionally related regions are identified by means of their synchronous slow fluctuations in signal intensity [20].

3.2.2.2 Clinical Applications of Rs-fMRI

For clinical studies, the resting state paradigm is appealing because it does not require sophisticated experimental setup and is suitable with uncooperative patient population. This can be performed on coma or anesthesia induced patients. Researchers are applying rs-fMRI scans to study various neurological and psychiatric disorders. The first clinical application of rs-fMRI was on Alzheimer's (AD) patients. Li et al., reported that AD patients have impaired functional connectivity in both hippocampi, compared to normal controls. This was correlated with the loss of cognitive ability [21]. Thus, rs-fMRI is used to obtain patient-specific diagnostic and prognostic information [22].

3.3 Resting State Networks

Resting state networks (RSNs) are localized to gray matter regions and reflect functional systems supporting perceptual and cognitive processes; they display a high level of correlated BOLD signal activity. The anatomical connections consist of white matter tracts that both directly and indirectly interconnect brain regions. Combining functional connectivity with diffusion tensor imaging (DTI), a MRI technique that allows the study of white matter fiber bundles, shows a direct association between functional and structural connectivity. Using ROI-based analysis and independent component analysis (ICA), eight major RSNs have been detected. The ROI based method requires a prior selection of a voxel or cluster. It provides a direct answer to direct question. ICA, on the

other hand, works by decomposing a two-dimensional data matrix into the time course and associated spatial maps of the underlying hidden signal. Similar to ROI method, ICA approach has identified networks of spontaneous coherence to known sensory and cognitive processing systems [23]. The key networks typically observed during rest include: DMN, the sensorimotor network, the executive control network, the auditory network, the temporal-parietal network, and up to three visual networks.

3.3.1 Default Mode Network

The most studied network during resting-state fMRI is DMN. In fMRI, the cognitive functions that are present in the DMN are linked to self-related and internal processes, such as stimulus independent thoughts, mind wandering, social cognition, and introspection. The DMN consists of signals that are identifiable in posterior cingulate cortex, lateral parietal cortex, and mesial prefrontal cortex [12]. These set of regions are activated during rest and relatively de-activated during task activity. This network was identified through seed-based correlation analysis. Spontaneous correlations have also been observed throughout the DMN across various states of altered consciousness, including sleep and anesthesia [24]. Decreased connectivity in the DMN reflects restricted abilities for self-referential processing in patients with disorders of consciousness.

3.3.2 Visual Network

The visual system consists of three different networks. The first network is characterized by the activity in mesial visual areas, striate cortex and extra-striate regions typically mesial, such as lingual gyrus. The second network is associated with lateral visual areas such as the occipital pole and occipital-temporal regions. The third network includes

activity in the striate cortex and in polar visual areas. Rs-fMRI studies have shown that resting-state BOLD fluctuations are controlled by a visual task performed prior to the data acquisition. This shows that resting-state BOLD fluctuations have dynamic components that are experience dependent and which may play a role in memory consolidation [12].

As stated in this section, there are many brain networks that play a major role in rs-fMRI experiment. These networks are also seen during a task stimulus fMRI experiment but the network that is observed is related to that specific task. ALFF and fALFF approaches look at the frequency-domain characteristic of the BOLD signals at rest.

CHAPTER 4

METHODS

4.1 Subject Information

In this experiment 22 healthy subjects were scanned. In total, there were 10 female and 12 male subjects. A Siemens 3.0 Tesla scanner equipped for EPI was used for data acquisition.

4.2 fMRI Data Acquisition

Two scans were performed for each subject. The first scan looked at the anatomical information, which was obtained from high-resolution MPRAGE images through T1 relaxation times. The second scan was the resting-state scan where the subjects were instructed to stare at the cross hair. All the subjects have the same baseline criteria; so eyes open or closed at rest should not affect the rs-fMRI analysis.

Each subject had resting-state data of 1000 continuous EPI functional volumes (TR = 2500ms; TE = 30ms; flip angle = 90 degrees; 34 slices, matrix = 80x80, field of view {FOV} = 240mm, slice thickness = 4mm, voxel size = 3x3x4mm). The resting-state scan for each subject lasted for 2500s. MPRAGE volume was acquired with acquisition matrix 256x256x144.

4.3 fMRI Data Pre-Processing

Different software packages are used for pre-processing steps in this study, including AFNI, FSL, and SPM8. Some of the pre-processing steps include realignment, co-registration, truncation of time points, de-oblique datasets, changing orientation of datasets, creating gray matter volume/segments, creating a functional to standard .mat file, transforming data sets from raw into standard space.

4.3.1 Realignment and Co-registration in SPM8

For this study, all subjects resting-state and MPRAGE fMRI data were pre-processed using SPM8, at tool box in MATLAB2011 [25]. The EPI images were corrected for motion related signal changes using the realignment tool in SPM8. This realigns a time-series of images acquired from the same subject using a least squares approach and 6 parameters. The parameters included 3 translations (x-, y-, & z- directions) and 3 rotations (roll, pitch, & yawn). These spatial transformations try to minimize the differences between each successive scan and a reference scan. The aim is to remove movement artifact in fMRI time-series data; however, the drawback of head motion is that the same voxel might represent different location of brain over time.

Once all the slices are corrected for head motion co-registration takes place. This step attempts to co-register the functional head motion corrected images and anatomical MPRAGE images for each subject in SPM8 [26].

4.3.2 Truncation of Original Time Series

Before the realigned and co-registered time series can be used for further pre-processing steps, the slices in the entire volume of the brain were de-obliqued using AFNI software package. FMRI EPI datasets are generally acquired in oblique pattern while anatomical datasets are in cardinal space. All datasets are transformed into orthogonal space, where the images are observed from three-axis coordinate system: axial, sagittal, and coronal plane. It is necessary to de-oblique the EPI datasets when transforming it to a standard MNI brain template.

4.3.2.1 Removal of T1 Saturation Effect

In order to account for the longitudinal relaxation time (T1) at the beginning of data acquisition, the first five time points from each subject were removed. This step was performed using fslori command in AFNI. All preprocessing steps try to increase contrast between network correlations and reduce nonspecific/noise correlations [6].

4.3.2.2 Calculation of Different Runs

After all the subjects had the same time series, 31 different runs were created starting with 32 time points with an increment of 32 time points going up to 992 time points for each subject, calculated in AFNI. Picking increments of 32 time points is essential for FFT calculations because the Cooley-Tukey (Butterfly) diagram only takes into account half of the data either sine or cosine component and the data has to be a power of two. The run scan time started at 1.33 minutes and ended at 41.33 minutes with a TR of 2.5 seconds. The goal of this study is to identify the minimum amount of time a healthy person needs to be in the scanner during a rs-fMRI scan, by detecting the spontaneous BOLD signal using two resting state properties from the frequency domain analysis (ALFF and fALFF).

4.4 Creating Functional to Standard Matrix

In order to convert the fMRI dataset into standard space, the new truncated time series was first deobliqued. Then the time series was converted to RPI (Right to Left, Posterior to Anterior and Inferior to Superior) format. Using the FLIRT command in AFNI the time series was converted to MNI152_T1_3mm_brain standard space template provided by FSL software (voxel size= 3x3x3 mm). This registers the fMRI time-series dataset to

MNI template for any type of analysis on this dataset. The Perl script to calculate the standard matrix is in APPENDIX A.

4.5 Extract Gray Matter Segment

The next pre-processing step was to get the gray matter segment for each subject from the preprocessed time-series and the MPRAGE images using AFNI. According to APPENDIX B, 3dvolreg specifies the processing step to be spatial realignment by taking the reference volume as mean_rREST and using interpolation technique as Fourier interpolation and does two passes of the registration algorithm. Using MPRAGE images from each subject and converting it to NIFTI format creates three different segments of the brain; white matter, gray matter, and cerebral spinal fluid (csf). The gray matter segment is created with a 0.7 threshold.

The gray matter segment is now converted to standard space using the standard space MNI template provided by FSL software incorporating the previously created func2std.mat file. This process involved a 3-step process: first, a 6 degree of freedom linear affine transformation was carried out using FLIRT to align the functional data into structural space. The anatomical image of the gray matter mask was then aligned to the standard MNI152 space using a 12 degree of freedom linear affine transformation using FLIRT [27].

4.6 ALFF and FALFF Calculation

As previously mentioned, this thesis looks in to the amplitude information of the BOLD signal and not the signal itself for connectivity patterns. For each subject, to measure the properties of amplitude of low frequency fluctuations at each voxel two common approaches were measured: ALFF and fALFF.

4.6.1 ALFF Calculations

ALFF analysis was done on the frequency information of the BOLD signal using REST toolbox in MATLAB2011. It measures the strength and intensity of LFO amplitudes. To get ALFF measures at each voxel, the time series for each voxel was filtered (band-pass, 0.01-0.8 Hz) to remove the effects of very low-frequency drift and high frequency noise. Next, the filtered time series was then transferred to the frequency domain by FFT. The power spectrum was then computed by squaring the amplitude at each frequency. Then the square root of the power spectrum was calculated for each voxel at each frequency range across 0.01-0.08 Hz. Finally, the average square root was taken across 0.01-0.08 Hz as the ALFF measurement for each single voxel. To get better measure of ALFF values at each voxel, the mean ALFF (mALFF) was calculated by dividing the whole brain ALFF measures at each voxel. ALFF can clearly distinguish between gray matter and white matter because these LFF are better detectable within gray matter [18].

4.6.2 FALFF Calculations

Similarly, to improve the original ALFF approach, a ratio of the power of each frequency at the low-frequency range (0.01-0.08 Hz) to that of the entire frequency range (0-0.2 Hz) was used. The sampling rate for this study is 0.4 Hz (1/TR=1/2.5 secs). This was again calculated using the REST toolbox in MATLAB2011. The time series of each voxel was transformed to a frequency domain. The square root was calculated at each frequency of the power spectrum. Finally, the sum of amplitude across 0.01-0.08 Hz was divided by that across the entire frequency range (0-0.2Hz). This value is known as the fALFF values at each voxel [28]. FALFF measures the relative contribution of specific LFO to the whole frequency range and it can provide a more specific measure of LFO.

However, the total energy of the signal may be different across brain regions (voxels), which can lead fALFF to differ from ALFF in some regions more than others [18].

4.6.3 Conversion into Standard Space Maps

In order to perform various analyses on this dataset, the mALFF maps and fALFF maps were further pre-processed. The maps were first converted to NIFTI (.nii) format in AFNI and then converted to standard space map using the func2std matrix previously created. The matrix now becomes 61x73x61 and the voxel size 3x3x3mm for each run. This is described in APPENDIX C.

4.7 Gray Matter Masks

For the gray matter mask, for each run, the mALFF maps and the gray matter segment were multiplied to get a 3D mask of just the gray matter mALFF voxel values. The MATLAB2011 script is in APPEDIX D. The fALFF values are within one and the mALFF values range from 0.3 to 9.0 to illustrate the mALFF values at each voxel, figure 4.1.
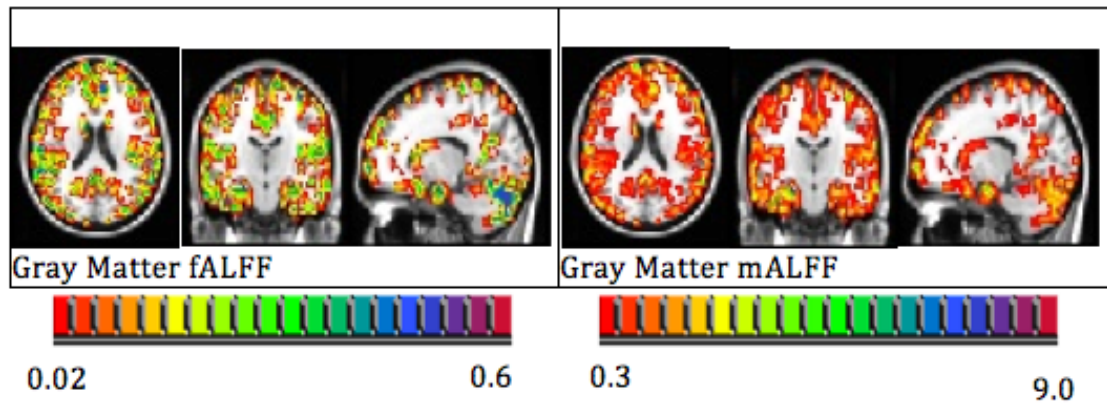

Figure 4.1 GM mask at rest with axial, coronal, and sagittal brain-views. (fALFF (L) ; mALFF (R)).

4.8 Pearson's Correlation Coefficient

Correlation is a statistical procedure to measure the degree of similarity between two different sets of data. The correlation value between any two sets of data ranges from -1 to 1. In this study, the correlation value measure between two fALFF/mALFF spatial maps in an ROI comparing two consecutive runs was positive. Pearson's correlation coefficient r-values were calculated using corr2 function in MATLAB2011 for each time point's voxel. After the gray matter mask for each run was calculated, the 3D mALFF and fALFF spatial maps were reshaped to 1D maps and all the nonzero values were extracted for correlation calculation. APPENDIX E describes the MATLAB2011 script for calculating gray matter r-values. Similar script was used to calculate whole brain correlation values on the standard space mALFF and fALFF spatial maps.

4.9 Independent Component Networks (ICNs) Calculation

During rs-fMRI, the brain activates a number of networks described by coherent neuronal LFOs from 0.01-0.08 Hz. This study looks into the DMN and the visual state network at rest. The 6 different standard space IC masks were calculated by Beckhman et. al [29]. The authors generated these masks using the probabilistic independent component analysis (PICA) approach. The specific IC masks were used from Taylor et al., where they identified what each component corresponds to in the RSNs. The IC masks used were 1,2,3 (visual network) and 5,6,13 (DMN) [30]. The mask calculation was similar to the gray matter masks previously described. Pearson's correlation coefficient was again calculated from each successive run for each of the 22 subjects. Figures 4.2 and 4.3 illustrate regions activated by specific IC mask.
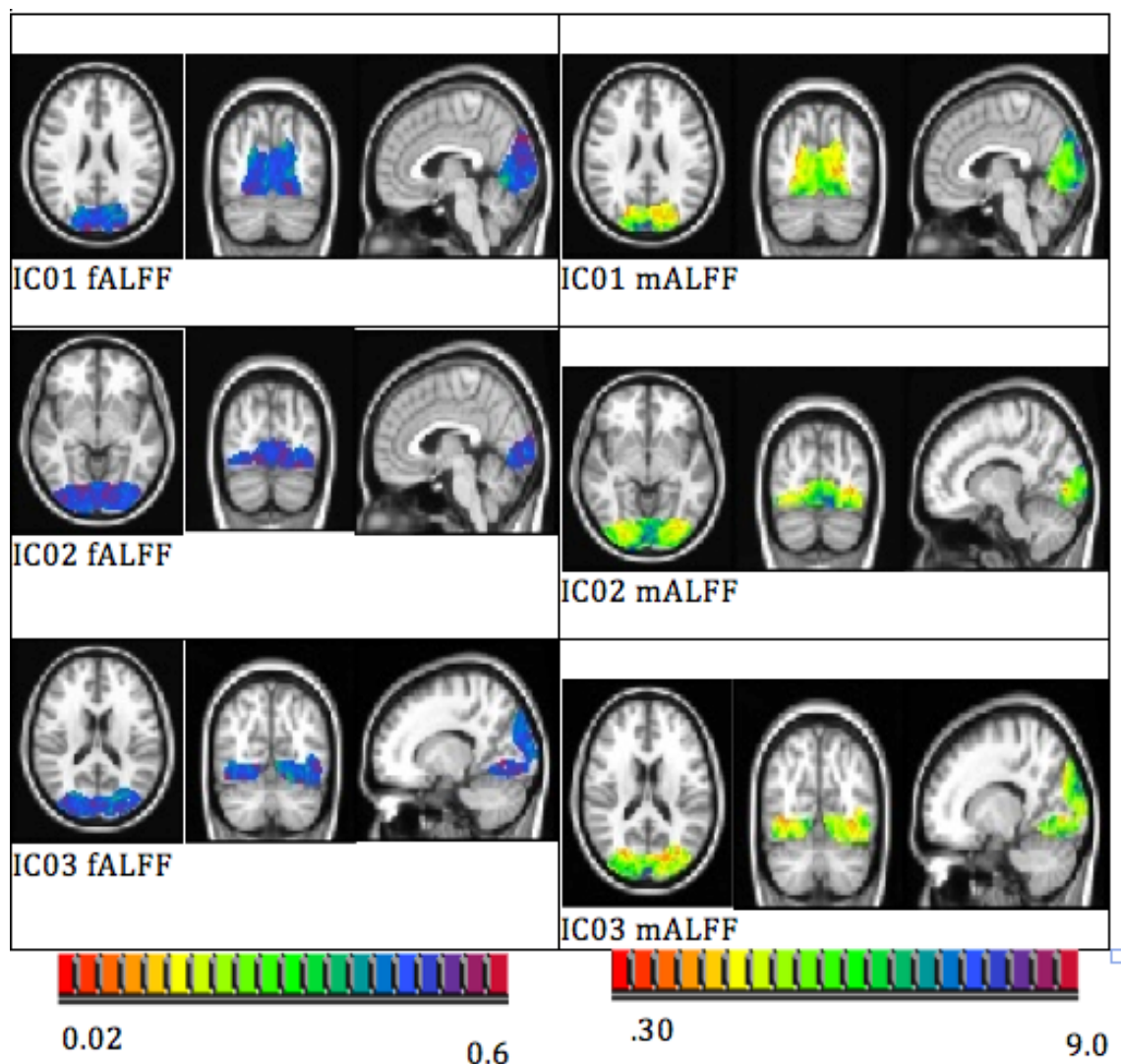
Figure 4.2 Three different IC masks that represent the visual network at rest with axial, coronal, and sagittal brain-views. (fALFF (L); mALFF (R))
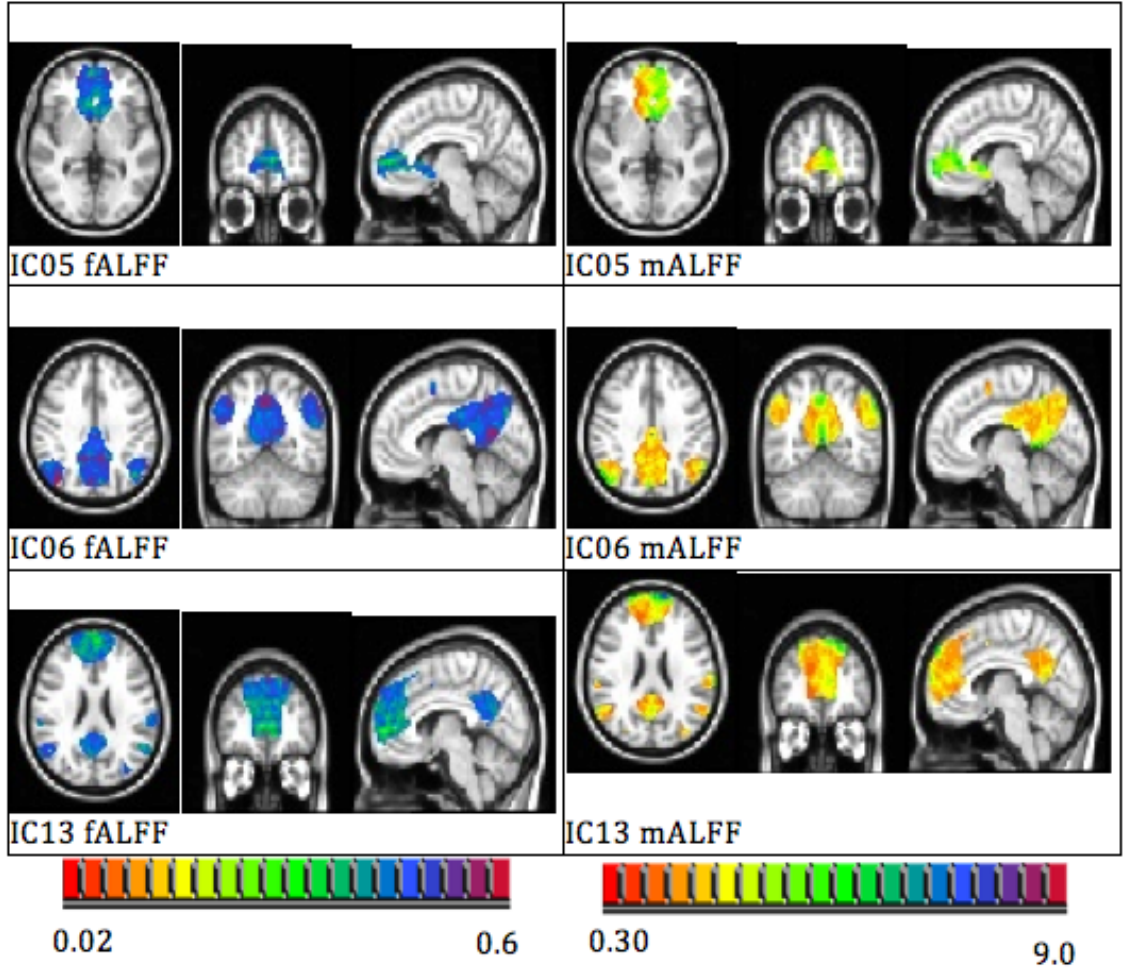
Figure 4.3 Three different IC masks that represent the DMN at rest with axial, coronal, and sagittal brain-views. (fALFF (L); mALFF (R))

4.10 Time Calculation

Once all the Pearson's correlation coefficients were generated for each subject from whole brain, gray matter, and the 6 different ICs minimum resting state scan time was calculated. To calculate the time across all 22 subjects, all the r-values were transformed to fisher's z scores, equation 4.1.

$$Z=0.5 * \ln [(1+r) / (1-r)] \tag{4.1}$$

4.10.1 Group Level Analysis Based on Pearson's Correlation Coefficient

Using the Pearson's correlation coefficients r- values at each run (30) across 22 subjects, the minimum resting-state scan time was obtained. This was done by plotting all the 22 subjects r-values for whole brain ROI and eyeing when the lines asymptote to a steady point.

4.10.2 Group Level Analysis Based on Fisher's Z Transformation

The mean across each run was calculated across 22 subjects z-scores. Using MATLAB2011 curve fitting toolbox, an exponential curve fit was fit to the data. This type of model represented the curve for the mean values, equation 4.2.

$$F (x) = a*exp^\wedge (b*x) + c* exp ^\wedge (d*x) \qquad\qquad (4.2)$$

Once all the mean values were fit to equation 4.2, tau (time constant) was calculated. This is the time it takes the system's step response to reach $1-1/e = 63.2\%$ of its final value using the values derived from equation 4.2. This type of model best characterizes the asymptote in the plot. This quantifies the ideal resting state scan time for 22 healthy subjects to detect the amplitude information in BOLD signal.

4.10.3 Inter-subject Analysis using Z-Scores

Lastly, to look at the minimum scanner time within a subject, the z-score values were used. Again fitting the z-values at each run within a subject on to equation 4.2 and calculating the tau constant, identified the minimum resting-state scan time for each individual. The results from all the analysis are descried in the next chapter.

CHAPTER 5

RESULTS

5.1 Overview of Results

This chapter summarizes all the results that were acquired after the pre-processing and post processing steps in SPM8, AFNI, REST, and FSL programs. The goal of this study was to figure out the minimum amount of time necessary to detect a stable resting state fALFF and mALFF values for the whole brain analysis or for the different ROIs. Thirty-one runs were calculated from the pre-processed time series. The Pearson's correlation coefficients (r-values) were calculated with each consecutive subsection's spatial mALFF and fALFF map. For example, an r-value was calculated between time-points 32-64 (run 1), time-points 64-96 (run 2)…etc. There were 30 r-values for each subject. In this manner, the scanner time started from 2.666 minutes and went up to 41.333 minutes. Once the correlation values were calculated for each run, the minimum time would then depend on whether the values drastically changed from run 1 or run 2. If the values did not change, from 32-64 to 64-96, then one can conclude that the minimum resting-state time point/ minutes correspond to the 64th time point. Last, Fisher's z transforms from each subject's r-value were calculated. Two forms of analysis were done, within subject and across subject. Using two models to model the system, the minimum resting state scan time was obtained.

5.1.1 Group Level: Pearson's Correlation Coefficient Analysis

Prior to calculating fisher z-scores for every subject's r-values, Pearson's correlation coefficient r-values were plotted for the 22 subjects on one plot and the minimum resting

state scan time across the 22 subjects was then calculated. To calculate the minimum time across the 22 subjects, the time when most of the r-values stabilized to a steady r-value was examined. So choosing the resting state scan time above the desired time only states that the mALFF and fALFF values in the BOLD signal would not vary as much. Thus, the fALFF and mALFF values have stabilized to steady a number at the desired time. Figure 5.1 illustrates the Pearson's correlation coefficient r-values across 22 subjects for gray matter. The x-axis represents the 30 different runs converted to minutes using TR = 2.5 s. The y-values are the r-values at each run. As is evident from the graph, the minimum r-value starts at 0.9 and goes to .99 and the lines stabilize very quickly as can be observed from the steep slope.
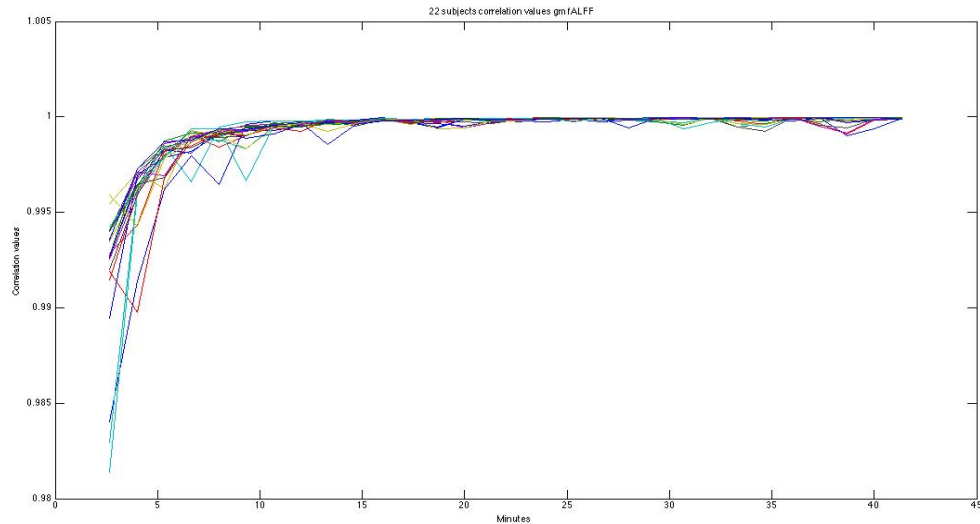
Figure 5.1 Gray Matter fALFF Correlation Coefficient R values across 22 subjects

According to Tables 5.1 and 5.2, mALFF signals take less time to detect at resting state for whole brain & gray matter and even significantly less time to detect the different IC networks at rest. A similar trend is shown for fALFF analysis. However, this is just by eyeing the correlation coefficients at rest and picking the length required. Thus, this is not the best way to look at the correlation values.

Table 5.1- Pearson's Correlation Coefficient - mALFF analysis

	Time (minutes)	Time Point
Whole Brain	5.333	96
Grey Matter	5.333	96
IC01	6.667	128
IC02	6.667	128
IC03	6.667	128
IC05	6.667	128
IC06	6.667	128
IC13	6.667	128

Table 5.2- Pearson's Correlation Coefficient - fALFF analysis

	Time (minutes)	Time Point
Whole Brain	6.667	128
Grey Matter	6.667	128
IC01	10.667	224
IC02	10.667	224
IC03	10.667	224
IC05	10.667	224
IC06	10.667	224
IC13	10.667	224

5.1.2 Group Level Analysis on Fisher's Z Transformation

To get a better visualization of the r-values, the Fisher's z transformation was performed to get z-values for each r-value for each subject. When performing group level analysis, the mean was calculated across all the z-values from each subject's run. The total mean values across 22 subjects were 30. To understand what the values mean, two different fits were performed. Figure 5.2 shows the plot of the scattered mean values across 22 subjects on the y-axis, and the x- axis represents the minutes associated with each run. The solid blue line was the exponential fit that was calculated using the curve fitting toolbox in MATLAB2011. The curve asymptotes after a certain time, and to represent what time, the exponential decay model was referenced. When the mean value reached 63.2% of its final value represented by the exponential fit model, the time in this case

would represent the desirable scanner time for healthy subjects' mALFF and fALFF values at rest.
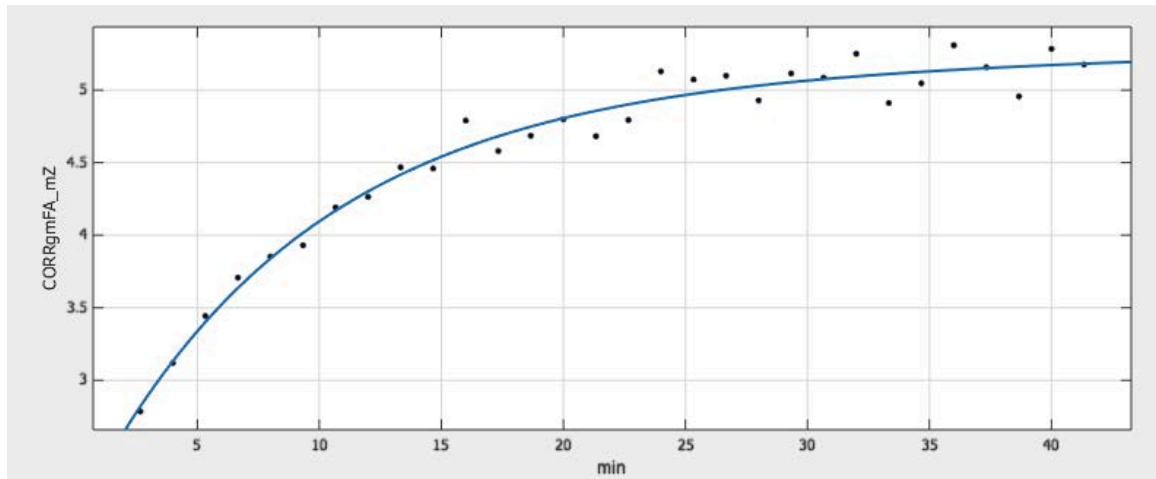
Figure 5.2 Gray Matter fALFF (r-values-> z-scores -> mean of z-scores across 22 subjects-> curve fit)

Tables 5.3 and 5.4 describe the minimum amount of rs-fMRI scanner time needed to reliably detect mALFF and fALFF signals for whole brain and different regions of interest. The results show that the correlation values stabilize around 13 minutes across 22 healthy subjects. This may be due to the fact that the correlation coefficients are not directly related to pre-processed data to detect functional connectivity but on the amplitude of the BOLD signal at rest.

Table 5.3 mALFF Analyses:
Equation to fit:

$$F(x) = a*exp(b*x) + c*exp(d*x)$$

Coefficient Values for each variable:

Regions/Masks	A	B	C	D	Time point	Time (minutes)
Whole Brain	4.0	-0.0004	-2.9	-0.09	288	13.33
Gray Matter	5.0	0.0005	-2.9	-0.11	256	12
IC 01	3.6	0.00009	-2.9	-0.08	288	13.33
IC 02	3.7	-0.003	-3.5	-0.08	256	12
IC 03	3.7	-0.002	-3.3	-0.08	288	13.33
IC 05	2.9	0.001	-2.4	-0.09	288	13.33
IC 06	3.7	-0.0007	-3.1	-0.08	288	13.33
IC 13	3.2	0.0004	-2.8	-0.09	288	13.33

Table 5.4 fALFF Analyses:
Equation to fit:

$$F(x) = a*exp(b*x) + c*exp(d*x)$$

Coefficient Values for each variable:

Regions/Masks	A	B	C	D	Time point	Time (minutes)
Whole Brain	4.0	0.004	-2.9	-0.15	256	12
Gray Matter	4.3	0.003	-2.8	-0.14	256	12
IC 01	3.8	0.004	-2.7	-0.14	288	13.33
IC 02	3.9	0.003	-2.8	-0.13	288	13.33
IC 03	3.7	0.003	-2.8	-0.14	256	12
IC 05	3.8	0.004	-2.8	-0.12	288	13.33
IC 06	3.5	0.005	-2.6	-0.16	256	12
IC 13	3.5	0.005	-2.7	-0.16	256	12

5.1.3 Inter-Subject Analysis

Finally, within subject analysis was performed on the calculated z-values for each subject. Again the curve fitting toolbox was used to calculate the minimum resting state scan time within a subject. There were 30 z-values for each subject corresponding to their r-values. Figure 5.3 illustrates a bar plot of how the 14 selected subjects show variability in detecting their desirable scan time to reliably identify the fALFF and mALFF signals at rest. The rest 8 subjects were excluded from this analysis because their z-values did not

fit to the specified curve. The variability among 14 subjects should exist because no two

people have the same brain structure or BOLD signals at rest.
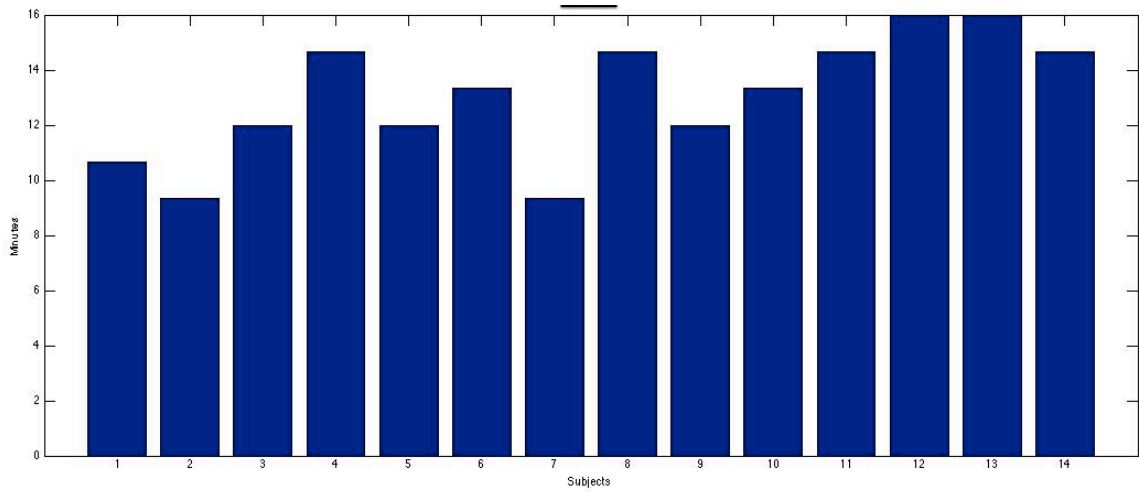
Figure 5.3 Bar plot of 14 subjects gray matter fALFF z-values

From table 5.5 one can notice that looking at r-values (table 5.1 & 5.2) will give you a

shorter scan time compared to z-values for each individual. The minimum scanner time

ranged from 9 to 16 minutes for 14 individual subjects.

Table 5.5 fALFF Analyses: 30 z-scores within a subject – gray matter
Equation to fit the 30 z-scores:

$$F(x) = a*exp(b*x) + c*exp(d*x)$$

Coefficient Values for each variable:

Subject	A	B	C	D	Time point	Minutes
1	4.8	0.002	-3.8	-0.15	224	10.66
2	5.0	0.002	-3.3	-0.19	192	9.33
4 (removed 4 outliers)	4.6	0.005	-3.3	-0.16	256	12
6	4.4	0.006	-2.6	-0.16	320	14.66
8	4.0	0.0057	-2.7	-0.24	256	12
10	4.7	0.0028	-2.7	-0.12	288	13.33
13	5.2	-0.0013	-3.1	-0.12	192	9.33
17	4.3	0.007	-3.0	-0.16	320	14.66
18	4.23	0.007	-3.65	-0.25	256	12
21	4.48	0.004	-2.6	-0.145	288	13.33
22	5.6	-0.0012	-3.2	-0.07	320	14.66
12	4.7	0.0048	-2.7	-0.12	352	16
9	4.1	0.007	-2.3	-0.21	352	16
5	5.1	0.001	-2.7	-0.08	320	14.66

CHAPTER 6

DISCUSSION

The results derived from this study can be used for most fMRI resting-state scans because the TR of 2.5 seconds is very popular in this field. The results indicate the minimum resting state scan time across 22 healthy subjects to vary from 9 to 16 minutes. This variation in detecting the ideal mALFF and fALFF measurements show that most of the noise might not have been regressed out in the pre-processing steps to account for such high values for Pearson's Correlation Coefficients. The ideal next step would be to re-perform this analysis but with modified pre-processing steps. This could lower the range of minimum resting state scan time.

A similar study on the resting state was performed by Van Dijk et al. [6], where they calculated the minimum time to detect functional connectivity in the brain at rest using incremental durations of scan time ranging from 2 to 12 minutes for six participants. They found that average correlation strengths between default, attention, and reference networks stabilized after using ~5 minutes of data. This suggested that multiple distinct correlation strengths could be obtained as little as 5 minutes. This property of correlating specific brain regions is another parameter that the rs-fMRI BOLD signal can be used to analyze.

The results from this current study show that no matter what part of the brain one is trying to analyze the minimum scanner time is approximately the same. Even though these results only pertain to the study at hand, this could be used as a basis for future studies. The next step in this study would be to look at the other ICNs and calculate the minimum scanner time and see how much the minutes vary by. Once different networks

are calculated in healthy subjects, it may be appropriate to look into patients suffering from neurological disorders and describe the trend in that particular disorder. The hypothesis stated at the beginning was proven to be correct because it stated that there is a desired resting-state scan time when looking at BOLD signals from rs-fMRI studies to get acceptable values of fALFF and mALFF values in healthy brain. This suggests that the data acquired after this optimal time does not give one a huge change in their mALFF and fALFF values because the results indicates that these values indeed do level off after certain time to become asymptotic.

APPENDIX A

SCRIPT FILE TO CONVERT RAW DATA INTO STANDARD MATRIX

This matrix is used to convert all the maps into standard space.

```perl
#!/usr/bin/perl
@sublist=('LF1', 'LF2', 'LF3', 'LF4', 'LM1', 'LM2', 'LM3', 'LM4', 'LM5', 'LM8', 'RF1',
'RF2', 'RF3', 'RF4', 'RF5', 'RF6','RM1', 'RM2', 'RM3', 'RM4', 'RM6', 'RM7');

for($i=0;$i<22;$i++)
{
        $subname=@sublist[$i];

$path = "/home/paul/prerpro3_11/"."$subname";
chdir "$path";
print "$path\n";


`3drefit -deoblique cut_rREST_40min.nii`;
`3drefit -deoblique MPRAGEskstrip.nii.gz`;
# convert it to RPI
`3dresample    -orient    RPI    -prefix    reor_cut_rREST_40min.nii    -inset
cut_rREST_40min.nii`;
`3dresample    -orient    RPI    -prefix    reor_MPRAGEskstrip.nii.gz    -inset
MPRAGEskstrip.nii.gz`;
# 1st transformaltion
`flirt            -in            reor_MPRAGEskstrip.nii.gz            -ref
/usr/share/fsl/data/standard/MNI152_T1_3mm_brain.nii.gz -omat struct2standard.mat`;
`flirt            -in            reor_MPRAGEskstrip.nii.gz            -ref
/usr/share/fsl/data/standard/MNI152_T1_3mm_brain.nii.gz -omat struct2standard.mat -o
mprage_mni`;
`flirt    -in    reor_MPRAGEskstrip.nii.gz    -ref    reor_cut_rREST_40min.nii    -omat
struct2func_13.mat`;
# convert_xfm convert_xfm (Version 2.1)
`convert_xfm -omat func2struct.mat -inverse struct2func_13.mat`;
`convert_xfm -omat func2std.mat -concat struct2standard.mat func2struct.mat`;
`flirt            -in            reor_cut_rREST_40min.nii            -ref
/usr/share/fsl/data/standard/MNI152_T1_3mm_brain.nii.gz -applyxfm -init func2std.mat
-o reor_cut_rREST_40min_mni3.nii`;

}
```

APPENDIX B

SCRIPT USED TO CREATE GRAY MATTER SEGMENT

The different segments are created to use as future masks.

```perl
#!/usr/bin/perl

@sublist=('LF1', 'LF2', 'LF3', 'LF4', 'LM1', 'LM2', 'LM3', 'LM4', 'LM5', 'LM8', 'RF1',
'RF2', 'RF3', 'RF4', 'RF5', 'RF6','RM1', 'RM2', 'RM3', 'RM4', 'RM6', 'RM7');

for($i=0;$i<22;$i++)
{
        $subname=@sublist[$i];

$path = "/home/paul/prerpro3_11/"."$subname";
chdir "$path";
print "$path\n";

# look at the cut rREST with 995 tr 2.5
`3dTstat -prefix mean_rREST_40min.nii.gz  cut_rREST_40min.nii`;

 `3dvolreg  -base  mean_rREST_40min.nii.gz  -fourier  -twopass  -1Dfile  motion.1D
cut_rREST_40min.nii`;

`bet2 MPRAGE.nii MPRAGEskstrip.nii.gz`;
`3dAFNItoNIFTI -prefix volreg.nii.gz volreg+orig.`;
`flirt -in MPRAGEskstrip.nii.gz -ref volreg.nii.gz -omat struct2func.mat -interp trilinear`;
`flirt -in MPRAGEskstrip.nii.gz -ref volreg.nii.gz -o mprage2func.nii.gz -applyxfm -init
struct2func.mat -interp trilinear`;
# creates 3 segments
`fast -g -p -o seg MPRAGEskstrip.nii.gz`;
# gray matter--create just this,detrends the time series
`flirt -in seg_prob_1.nii.gz -ref volreg.nii.gz -o mprage2func_seg1.nii.gz -applyxfm -init
struct2func.mat -interp trilinear`;

$cmd="3dcalc  -a  mprage2func_seg1.nii.gz  -expr  "."'"."astep(a,0.70)"."'"."  -prefix
mask_seg1_311.nii.gz";
system($cmd);
`3dmaskdump -noijk -mask mask_seg1_311.nii.gz volreg.nii.gz > GM_time_311.1D`;

`3dDetrend   -DAFNI_1D_TRANOUT=YES   -prefix   GM_detrend_311   -polort   3
GM_time_311.1D`;
`gunzip  "$path"/mask_seg1_311.nii.gz`;

}
```

APPENDIX C

SCRIPT TO CONVERT SPATIAL MAPS TO STANDARD SPACE

Raw space images are converted to standard space for further analysis.

```perl
#!/usr/bin/perl

@sublist=( 'LF1', 'LF2', 'LF3', 'LF4', 'LM1', 'LM2', 'LM3', 'LM4', 'LM5', 'LM8', 'RF1',
'RF2', 'RF3', 'RF4', 'RF5', 'RF6','RM1', 'RM2', 'RM3', 'RM4','RM6','RM7');

@sublist2=('run_032',          'run_064',          'run_096',          'run_128','run_160',
'run_192','run_224','run_256','run_288','run_320','run_352','run_384',
'run_416','run_448','run_480','run_512','run_544','run_576','run_608','run_640',
'run_672','run_704','run_736','run_768','run_800','run_832','run_864','run_896','run_928','
run_960','run_992');

foreach($i=0;$i<22;$i++)
{
$subname=@sublist[$i];
$path = "/media/DATAPART1/dp-umd/prepro2/"."$subname";
chdir "$path";
print "$path\n";
foreach($j=0;$j<31;$j++)
{
$subname2=@sublist2[$j];
$path2 = "/media/DATAPART1/dp-umd/prepro2/"."$subname"."/"."$subname2";
 chdir "$path2";
print "$path2\n";
#all the maps in RPI convert from hdr to .nii (raw space).

#`3dcopy mALFF_MAP.hdr mALFF_13.nii`;
#`flirt -in mALFF_13.nii -ref /usr/share/fsl/data/standard/MNI152_T1_3mm_brain.nii.gz
-applyxfm -init $path/func2std_13.mat -o mALFF_13_mni3.nii`;
#`gunzip mALFF_13_mni3.nii.gz`;
#}
#}

#all the maps in RPI convert from hdr to .nii (raw space).
`3dcopy FALFF_MAP.hdr FALFF_13.nii`;
`flirt -in FALFF_13.nii -ref /usr/share/fsl/data/standard/MNI152_T1_3mm_brain.nii.gz -
applyxfm -init $path/func2std_13.mat -o FALFF_13_mni3.nii`;
`gunzip FALFF_13_mni3.nii.gz`;
}
}
```

APPENDIX D

CODE TO CREATE THE DIFFERENT ROI MASKS

The ROI masks are used to look at the time variability across brain.

```
close all
clear all

sfolder='/media/DATAPART1/dp-umd/prepro2/';
  S = dir([sfolder]);
  S=S(9:end);

for i=1:length(S)
   subdir=([sfolder, S(i).name]);    %goes in subject directory
   cd(subdir);
   D=dir([subdir]);
   D=D(16:end);

 for j=1:length(D)
   subdir2=([sfolder  S(i).name '/' D(j).name]);
   cd(subdir2); % directory where my alff maps are...
   RunTmp1=load_untouch_nii('mALFF_13_mni3.nii');  %  (3D) standard space maps
   RunTmpImg1=RunTmp1.img;
   RunTmp2=load_nii('maskseg1_13_mni3.nii'); % (3D) gm segment in standard space
   RunTmpImg2=RunTmp2.img;

% calc mask
 gm13ALFF=(RunTmpImg1.*RunTmpImg2); % multiplied both to get 3D mask of gm

varname='gm13ALFF';
 save (varname, 'gm13ALFF')

 end
 end
```

CODE TO CALCULATE PEARSON'S CORRELATION COEFFECIENT

Code to create correlation between runs.

```
close all
clear newdata newdata2

sfolder='/media/DATAPART1/dp-umd/prepro2/';
S = dir([sfolder]);
S=S(10);        % goes through all the subjects however right now its just set at one subject
Subjectcorr=[];   %This will become a columnar vector of each subjects COOR2 values

 for i=1:length(S)
   subdir=([sfolder, S(i).name]);      %goes in subject directory
   cd(subdir);
   D=dir([subdir]);
   D=D(16:end);          % goes in all the runs directory

for j=1:length(D)-1       % picks one run--consecutive
   subdir2_run1=([sfolder  S(i).name '/' D(j).name]);
   cd(subdir2_run1);

% loads the mask      --picks the map to correlate
 RunTmp=load ('gm13FALFF');      % could be either gmALFF/gmFALFF/ IC_FALFF
   RunTmpImg1D=reshape(RunTmp.gm13FALFF,1,61*73*61);  %  61*73*61
   ind=find(RunTmpImg1D);

for k=1:43383
     newdata(:,k)=RunTmpImg1D(:,ind(k));
   end

%different directory/diff run to compare with the run already picked.
 subdir2_run2=([sfolder  S(i).name '/' D(j+1).name]);       % consecutive run
 cd(subdir2_run2);        % changes directory to the next consecutive run

%loads the mask --picks the map to correlate with the other map
   RunTmp2=load ('gm13FALFF');        % could be either gmALFF/gmFALFF
   RunTmpImg1D_2=reshape(RunTmp2.gm13FALFF,1,61*73*61);      % reshapes the
vector from 3D map to 1D map.
   ind2=find(RunTmpImg1D_2);

 for l=1:43383
     newdata2(:,l)=RunTmpImg1D_2(:,ind2(l));
```

```matlab
   end


%calculates CORR2 between 2 consecutive runs
 SubCorrtmp=corr2( newdata,  newdata2);     % calculates corr2 two runs within a subject

%Group Subject data - allocation controlled by first loop "j"
    Subjectcorr(i,j)=SubCorrtmp;      % for every i and every j.
%[Z,mu,sigma] = zscore(Subjectcorr);  % gets the mean and z-scores for Corr values.

 end
 end
```

REFERENCES

1.   *Research*. Neuroimaging 2008 April 30,2013]; Available from: http://flavor.monell.org/~jlundstrom/research neuroimaging.html.

2.   M.H. Lee, C.D.S., J.S. Shimony, *Resting-State fMRI: A Review of Methods and Clinical Applications.* American Journal of Neuroradiology, 2012.p. 1-7.

3.   De Luca M, B.C., De Stefano N, Matthews PM, Smith SM fMRI resting state networks define distincy modes of long-distance interactions in the human brain. NeuroImage, 2006. **29**(4).

4.   Yeo BT, K.F., Sepulcre J, Buckner RL, Liu H, Sabuncu MR, Lashkari D, Hollinshead M, Roffman JL, Smoller JW, Zollei L, Polimeni JR, Fischl B, *The organization of the human cerebral cortex estimated by intrinsic functional connectivity.* Journal of Neurophysiology, 2011. **106**(3): p. 1125-65.

5.   Zhiqiang Zhang, W.L., Xi-Nian Zuo, Zhengge Wang, Bharat B. Biswal, et al., *Resting-State Brain Organization Revealed by Functional Covariance Networks.* PLoS ONE, 2011. **6**(12).

6.   Koene R. A. Van Dijk, T.H., Archana Venkataraman, Karleyton C. Evans, Sara W. Lazar and Randy L. Buckner, *Intrinsic Functional Connectivity As a Tool for Human Connectomics: Theory, Properties, and Optimization.* Journal of Neurophysiology, 2010. **103**: p. 297-321.

7.   Ellard, D. *History of MRI*. 2012 April 30,2013; Available from: http://www.isbe.man.ac.uk/personal/dellard/dje/history_mri/history of mri.htm.

8.   Joseph P. Hornak, P.D., *The Basics of NMR*. Vol. v. 1997-2011.

9.   Davison, J.E., Multimodal magnetic resonance investigation of childhood metabolic neurodegenrative disease, in School of Clinical and Experimental Medicine, College of Medical and Dental Sciences, University of Birmingham2012.

10.   Suetens, P., *Fundamentals of Medical Imaging*, in *Fundamentals of Medical Imaging*. 2009, Cambridge University Press: New York, NY USA.

11.   Scott A. Huetttel, A.W.S., Gregory McCarthy, *Functional Magnetic Resonance Imaging*. Vol. 1. 2004, Sunderland, Massachusetts, U.S.A.: Sinauer Associates, Inc.

12.   Cristina Rosazza, L.M., Resting-state brain networks: literature review and clinical applications. Neurological Sciences, 2011.

13.   Ogawa S, L.T.M., Kay A.R, Tank D.W, *Brain magnetic resonance imaging with contrast dependent on blood oxygenation.* Proc Natl Acad Sci USA, 1990. **87**: p. 9868-9872.

14.   Xiaoping Hu, E.Y., *The story of the initial dip in fMRI.* NeuroImage, 2012. **62**(2): p. 1103-1108.

15. Bharat B. Biswal, S.S.K., Bart Rypma, Hemodynamic Scaling of fMRI-BOLD signal: Validation of low frequency spectral amplitude as a Scalability Factor. Magnetic Resonance Imaging, 2007. **25**(10): p. 1358-1369.

16. Bharat B. Biswal, J.S.H., F. Zerrin Yetkin, Victor M. Haughton, *Functioanl Connectivity in the Motor Cortex of Resting Human Brain Using Echo-Planar MRI.* MRM, 1995. **34**: p. 537-541.

17. Brin RM, D.J., Smith MA, Bandettini PA, Separating respiratory-variation-related flunctuations from neuronal-activity- related fluctuations in fMRI. NeuroImage, 2006. **31**(4).

18. Xi-Nian Zuo, A.D.M., Clare Kelly, Zarrar E. Shehzad, Dylan G. Gee, Donald F. Klein, F. Xavier Castellanos, Bharat B. Biswal, Michael P. Milham, *The Oscillating Brain: Complex and Reliable.* NeuroImage, 2010. **49**(2): p. 1432-1445.

19. Lucina Q. Uddin, A.M.C.K., Bharat B. Biswal, F. Xavier Castellanos, Michael P. Milham *Functional Connectivity of Default Mode Network Components: Correlation, Anticorrelation, and Causality.* Human Brain Mapping, 2007. **30**: p. 627-637.

20. Dietmar Cordes, V.M.H., et al., *Mapping Functioanally Related Regions of Brain with Functional Connectivity MR Imaging.* American Journal of Neuroradiology, 2000. **21**: p. 1636-1644.

21. Wang Z, Y.C., Zhao C, Qi Z, Zhou W, Lu J, He Y, Li K, Spatial patterns of intrinsic brain activity in mild cognitive impairment and Alzheimer's disease: a resting-state functional MRI study. Human Brain Mapping, 2011. **32**(10).

22. Lizette Heine, A.S., Francisco Gomez, Resting state networks and consciousness: Alterations of multiple resting state networks connectivity in physiological, pharacological, and pathological consciousness states. Psychology, 2012. **3**.

23. David M. Cole, S.M.S.a.C.F.B., Adavances and pitfalls in the analysis and interpretation of resting-state FMRI data. frontiers in Systems Neuroscience, 2010. **4**(8).

24. Greicius MD, K.B., Reiss AL, Menon V., Functioanl connectivity in the resting brain: a network analysis of the default mode hypothesis. Proc Natl Acad Sci USA, 2003. **100**(1).

25. Group, T.F.M., *SPM8 Manul*, 2012: Functional Imaging Laboratory Wellcome Trust Center for Neuroimaging Institute of Neurology, UCL.

26. Friston, K.J., *Introduction Experimental design and Statistical Parametric Mapping*. The Wellcome Dept. of Cognitive Neurology, University College London.

27. Jie Song, A.S.D., Timothy B. Meier, Dana L. Tudorascu, Svyatoslav Vergun, Veena A. Nair, Bharat B. Biswal, *Age-Related Differences in Test-Retest Reability in Resting-State Brain Functional Connectivity.* PLoS ONE, 2012. **7**(12).

28.   Qi-Hong Zou, C.-Z.Z., et al., An imporved approach to detection of amplitude of low-frequency fluctuation (ALFF) for resting-state fMRI: Fractional ALFF. Journal of Neuroscience Methods, 2008. **172**: p. 137-141.

29.   Christian F. Beckmann, M.D.J.T.D.a.S.M.S., *Investigations into resting-state connectivity using independent component analysis.* Philosophical Transactions of The Royal Society B, 2005. **360**: p. 1001-1013.

30.   Paul Taylor, S.G., Xin Di, Bharat Biswal, Functional covariance networks: obtaining resting state networks from intersubject variability. Brain Connectivity, 2012. **2**(4): p. 203-217.